ARTICLES

Quantum Mechanical Pressure-Dependent Reaction and Recombination Rates for O + OH → H + O_2, HO_2

Timothy C. Germann and William H. Miller*

Department of Chemistry, University of California, and Chemical Sciences Division, Lawrence Berkeley National Laboratory, Berkeley, California 94720

Received: January 29, 1997; In Final Form: April 14, 1997[⊗]

We extend recent flux−flux autocorrelation function methods for the direct computation of thermal reaction rate constants and unimolecular recombination rates to the case where both reaction and recombination are possible. Rather than a single transition state dividing surface, dividing surfaces are placed on both the reactant (r) and product (p) sides of the intermediate collision complex region. The thermal recombination rate expression then involves a flux cross-correlation function $C_{rp}(t)$ in addition to the usual autocorrelation function $C_{rr}(t)$, both of which are computed during a single quantum time propagation. This method is applied to the three-dimensional O + OH ⇌ H + O_2 ($J = 0$) reactions, employing parallel computation because of the necessary large basis (2^{18} grid points) and long propagation times (2−3 ps). Thermal rate constants (in the absence of recombination effects) are presented for $T = 500-2000$ K, using the *J*-shifting approximation to account for nonzero total angular momentum; good agreement is found with experimental measurements of both forward and reverse rate constants. Collisional recombination by a bath gas is included via the strong collision assumption, and rate constants for the competing O + OH reaction (H + O_2) and recombination (HO_2) channels are calculated as a function of collision frequency, i.e., pressure of the bath gas.

I. Introduction

A great deal of progress has been made in recent years[1−5] in one's ability to carry out rigorous quantum mechanical calculations of chemical reaction rates by using flux−flux time correlation functions.[6,7] The primary feature that makes this approach efficient is that one calculates the rate constant "directly", avoiding the need to solve the full state-to-state reactive scattering problem and then to average the resulting cross sections over the appropriate distribution of initial and final states. The approach has vestiges of transition state theory, and the efficiencies resulting therefrom, but it is an exact formulation.

It has also recently been shown[8] how a quantum mechanical version of the Lindemann mechanism[9] for collisional recombination

$$A + B \rightleftharpoons AB^* \tag{1.1a}$$

$$AB^* + M \rightarrow AB + M \tag{1.1b}$$

can be expressed in terms of the flux correlation function for the A−B collision (eq 1.1a) provided one uses the strong collision approximation (SCA) for the energy relaxation step (eq 1.1b). (It has also been shown[10] how this theory can be generalized to go beyond the SCA, but this requires more than just the flux correlation function for the A−B collision.) This formulation eliminates both the ambiguities that arise when one is required to identify the energies and lifetimes of individual resonances in the A + B ⇌ AB* collision process, and also unphysical features that appear in the collision lifetime approach.[11]

Two applications of this new quantum theory of recombination have been reported thus far: Qi and Bowman[12] treated the H + CO → HCO recombination; Mandelshtam *et al.*[13] carried out similar calculations for H + O_2 → HO_2 at energies below the threshold for the O + OH product channel. In both cases the quantum time evolution operators needed to construct the flux correlation functions (see below) were obtained by diagonalizing the Hamiltonian (including an absorbing potential in the asymptotic region) in an L^2 basis set.

In this paper we generalize the previous quantum theory of recombination to include both chemical reaction as well as recombination, i.e.,

$$A + BC \rightleftharpoons ABC^* \rightarrow AB + C \tag{1.2a}$$

$$ABC^* + M \rightarrow ABC + M \tag{1.2b}$$

One is thus able to describe simultaneously the recombination reaction (A + BC → ABC), the effect of pressure (of the bath gas M) on the exchange reaction (A + BC → AB + C), and the competition between the two.

Application of this theory is then made to the important reactions

$$O + OH \rightleftharpoons H + O_2$$

which are central to combustion processes, with the reverse reaction providing the key radical chain branching step.[14,15] The competition between these reactions and the recombination reactions

$$O + OH + M \rightarrow HO_2 \leftarrow H + O_2 + M$$

which act as chain termination steps, largely determines the

[⊗] Abstract published in *Advance ACS Abstracts,* July 15, 1997.

S1089-5639(97)00362-9 CCC: $14.00

second explosion limit.[15] These reactions are also of great interest in atomospheric chemistry because of the importance of the HO_2 radical in the catalytic removal of stratospheric ozone.[16]

Section II first describes the extension of the earlier quantum mechanical collisional recombination theory[8] for the case where both reaction and recombination are present. Rather than utilizing a single dividing surface as is customary for the usual flux−flux autocorrelation function, one needs to introduce dividing surfaces on both the reactant (r) and product (p) sides of the region defining the collision complex and to construct the r−p cross-correlation function as well as the usual (r−r) autocorrelation function. Section III describes the approach of Thompson and Miller[2] that we have used to evaluate the flux correlation functions; here, it is not necessary to diagonalize the complex Hamiltonian (which would be quite impossible) but only to propagate (via the split operator algorithm) a relatively small number of eigenvectors of the Boltzmannized flux operator, $e^{-\beta\hat{H}/2}\hat{F}e^{-\beta\hat{H}/2}$. Special considerations for application on massively parallel computers are also discussed and are very effective in this case because of the large size of the basis (2^{18} grid points) and long propagation times (2−3 ps). Section IV then presents results for the O + OH system. Although only calculations for zero total angular momentum have been performed, $J > 0$ rates may be included approximately with the J-shifting approximation,[17] enabling comparison with experimental measurements of both forward and reverse rate constants over the temperature range $T = 500-2000$ K. Pressure-dependent fall-off curves for the O + OH → HO_2 recombination rate, as well as the pressure-induced dampening of the forward and reverse reaction rate constants, are readily computed from the same pair of correlation functions.

Finally, it should be emphasized again that although the present approach does an excellent job of describing the first step in the Lindemann mechanism, i.e., the bimolecular dynamics in eq 1.1a or eq 1.2a, it treats the second (energy relaxation) step, eq 1.1b or eq 1.2b, via the comparatively primitive strong collision approximation. Though the SCA can be made more realistic by defining[18] the collision frequency ω as an effective (temperature and species dependent) frequency, one can only incorporate a more complete description of collisions with the third body M (akin to a classical master equation treatment[9c]) by going to the more sophisticated approach in ref 10.

II. Flux Correlation Approach to Thermal Reaction and Recombination Rates

To generalize the previous quantum version of the Lindemann mechanism for recombination (eq 1.1), it is useful (as before) to begin with a *classical* description of the processes, i.e., what would be done in a classical trajectory simulation. Referring to Figure 1 for the O + OH → H + O_2, HO_2 system, the classical rate constants for reaction H + O_2 and recombination (HO_2) are both given as averages of the reactant flux over a Boltzmann distribution of initial conditions for classical trajectories

$$k(T) = [Q_r(T)]^{-1}(2\pi\hbar)^{-f}\int d\mathbf{p}_1\int d\mathbf{q}_1\, e^{-\beta H(\mathbf{p}_1,\mathbf{q}_1)}\, F_r(\mathbf{p}_1,\mathbf{q}_1)P(\mathbf{p}_1,\mathbf{q}_1) \tag{2.1}$$

where $F_r(\mathbf{p}_1,\mathbf{q}_1)$ is the flux factor related to the reactant dividing surface s_r in Figure 1 and $P(\mathbf{p}_1,\mathbf{q}_1)$ is the probability of either reaction or recombination as the case may be. If $h_r(\mathbf{q})$ is the Heaviside (step) function that is 0(1) for positions $\mathbf{q}$ to the left (right) of the dividing surface s_r in Figure 1, then the flux factor

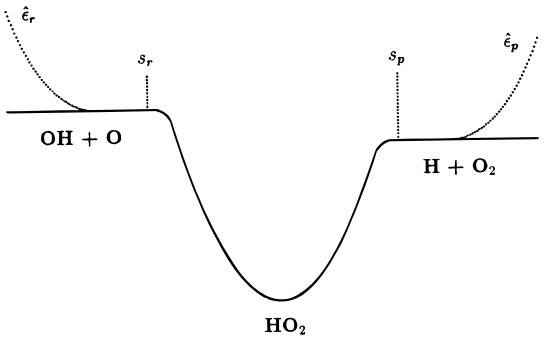

Figure 1. One-dimensional schematic diagram of the interaction potential for the O + OH → H + O_2 reaction versus reaction coordinate s. The HO_2 collision complex region is bounded by dividing surfaces on reactant (s_r) and product (s_p) sides, $s_r < s < s_p$.

F_r is given by

$$F_r = \frac{d}{dt}h_r(\mathbf{q}) = \frac{\partial h_r(\mathbf{q})}{\partial \mathbf{q}}\cdot\mathbf{p}/m \tag{2.2}$$

where the last equality applies only for Cartesian coordinates and momenta. Similarly, $h_p(\mathbf{q})$ is the Heaviside function that is 0(1) for positions $\mathbf{q}$ to the left (right) of the product dividing surface s_p. The difference of these two Heaviside functions,

$$h_c(\mathbf{q}) = h_r(\mathbf{q}) - h_p(\mathbf{q}) \tag{2.3}$$

is therefore 1 for positions $\mathbf{q}$ *between* the two dividing surfaces (i.e., in the "complex" region) and zero outside. Since $1 - e^{-\omega t}$ is the probability of the system experiencing a (deactivating) collision with the bath gas in the time interval $(0,t)$, the recombination probability is

$$P_{recomb}(\mathbf{p}_1,\mathbf{q}_1) = 1 - e^{-\omega\tau(\mathbf{p}_1,\mathbf{q}_1)} \tag{2.4a}$$

where $\tau(\mathbf{p}_1,\mathbf{q}_1)$ is the time the trajectory (having begun at $t = 0$ on s_r) exits the complex region. This can also be expressed as

$$P_{recomb}(\mathbf{p}_1,\mathbf{q}_1;\omega) = \int_0^\infty dt\, h_c(\mathbf{q}(t))\frac{d}{dt}(1 - e^{-\omega t}) \tag{2.4b}$$

which with an integration by parts becomes

$$P_{recomb}(\mathbf{p}_1,\mathbf{q}_1;\omega) = \int_0^\infty dt\,(e^{-\omega t} - 1)(F_r(t) - F_p(t)) \tag{2.4c}$$

(since $F_r(t) \equiv \frac{d}{dt}h_r(\mathbf{q}(t))$ and $F_p(t) \equiv \frac{d}{dt}h_p(\mathbf{q}(t))$). To have reaction, on the other hand, the trajectory must exit through dividing surface s_p and not have suffered a collision before it reaches it, i.e.,

$$P_{reaction} \equiv P_{p\leftarrow r}(\mathbf{p}_1,\mathbf{q}_1) = e^{-\omega\tau_p(\mathbf{p}_1,\mathbf{q}_1)} \tag{2.5a}$$

where τ_p is the time the trajectory exits through s_p. This can be written as

$$P_{p\leftarrow r} = \int_0^\infty dt\,(1 - h_p(\mathbf{q}(t)))\frac{d}{dt}e^{-\omega t} \tag{2.5b}$$

which with an integration by parts becomes

$$P_{p\leftarrow r} = \int_0^\infty dt\, F_p(t)e^{-\omega t} \tag{2.5c}$$

With the recombination and reaction proabilities given by eqs 2.4c and 2.5c, respectively, eq 2.1 gives the rate constants in terms of the flux correlation functions,

$$k_{\text{recomb}}(T) = [Q_r(T)]^{-1}\int_0^\infty dt\,(e^{-\omega t} - 1)(C_{rr}(t) - C_{rp}(t)) \tag{2.6a}$$

$$k_{p\leftarrow r}(T) = [Q_r(T)]^{-1}\int_0^\infty dt\, e^{-\omega t}C_{rp}(t) \tag{2.6b}$$

where

$$C_{rr}(t) = (2\pi\hbar)^{-f}\int d\mathbf{p}_1\int d\mathbf{q}_1\, e^{-\beta H(\mathbf{p}_1,\mathbf{q}_1)}F_r(\mathbf{p}_1,\mathbf{q}_1)F_r(\mathbf{p}_1,\mathbf{q}_1,t) \tag{2.7a}$$

$$C_{rp}(t) = (2\pi\hbar)^{-f}\int d\mathbf{p}_1\int d\mathbf{q}_1\, e^{-\beta H(\mathbf{p}_1,\mathbf{q}_1)}F_r(\mathbf{p}_1,\mathbf{q}_1)F_p(\mathbf{p}_1,\mathbf{q}_1,t) \tag{2.7b}$$

The transcription of eqs 2.6a and 2.6b to quantum mechanics simply involves replacing the classical flux correlation functions of eqs 2.7a and 2.7b by their quantum mechanical counterparts,

$$C_{rr}(t) = \text{Tr}[e^{-\beta\hat{H}/2}\hat{F}_r\, e^{-\beta\hat{H}/2}\, e^{i\hat{H}t/\hbar}\hat{F}_r\, e^{-i\hat{H}t/\hbar}] \tag{2.8a}$$

$$C_{rp}(t) = \text{Tr}[e^{-\beta\hat{H}/2}\hat{F}_r\, e^{-\beta\hat{H}/2}\, e^{i\hat{H}t/\hbar}\hat{F}_p\, e^{-i\hat{H}t/\hbar}] \tag{2.8b}$$

As in the previous case,[8] it is worth emphasizing that these correlation functions are properties of the isolated bimolecular reaction dynamics only and that the collision frequency ω enters only as a damping factor in the time integrals of these correlation functions (eq 2.6).

It is not hard to see that eqs 2.6a and 2.6b reduce to previous results in appropriate limits. For example, if the exchange reaction channel is closed, then $C_{rp}(t) \rightarrow 0$, and eq 2.6 reduces to the earlier quantum expression for the recombination rate. Also, in the limit of zero pressure (i.e., $\omega \equiv 0$), the recombination rate vanishes, and eq 2.6b, for the reaction rate is

$$\lim_{\omega\rightarrow 0} k_{p\leftarrow r}(T) = [Q_r(T)]^{-1}\int_0^\infty dt\, C_{rp}(t) \tag{2.9a}$$

$$= [Q_r(T)]^{-1}\int_0^\infty dt\, C_{rr}(t) \tag{2.9b}$$

where we have noted that the two dividing surfaces can be taken to be the same or different for an isolated bimolecular reaction. As will be seen in section IV, though, for cases where a long-lived collision complex is formed, as in the present example, use of eq 2.9a is more stable numerically, since it avoids cancellation of two large and approximately equal contributions. The equivalence of eqs 2.9a and 2.9b also means that the collisional factor $e^{-\omega t} - 1$ in eq 2.6a can formally be replaced by $e^{-\omega t}$, but for numerical stability it is better to stay with the original version.

Finally, we note that the earlier quantum recombination (but nonreactive) calculations by Qi and Bowman[12] and by Mandelshtam *et al.*[13] were carried out in a time-independent approach: the Hamiltonian plus a negative imaginary (absorbing) potential, $\hat{H} - i\hat{\epsilon}$, was diagonalized in an L^2 basis, the traces in eqs 2.8a and 2.8b carried out in the basis of these eigenfunctions, and the time integral in eqs 2.6a and 2.6b then (trivially) evaluated. Though we do not use this approach in our present calculations, the Appendix gives the appropriate formulas for such an approach to the reaction/recombination rates of eqs 2.6a and 2.6b.

III. Computational Details

A. Reaction Coordinates and HO_2 Potential Energy Surface. Jacobi coordiates for the H + O_2 arrangement are used, as shown in Figure 2. Here r is the O−O bond distance,

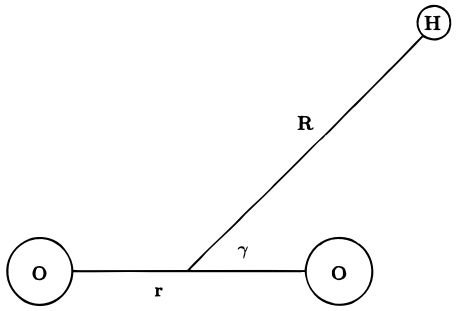

Figure 2. Jacobi coordinates for H + O_2.

R the distance between the H atom and O_2 center-of-mass, and γ the angle between **R** and **r**. In this coordinate system, the $J = 0$ Hamiltonian is given by

$$\hat{H} = -\frac{\hbar}{2\mu_R}\frac{\partial^2}{\partial R^2} - \frac{\hbar}{2\mu_r}\frac{\partial^2}{\partial r^2} + \left(\frac{1}{2\mu_R R^2} + \frac{1}{2\mu_r r^2}\right)\hat{\mathbf{l}}^2 + \hat{V}(R,r,\gamma) \tag{3.1}$$

where $\hat{\mathbf{l}}$ is the orbital angular momemtum operator for H rotation about the O_2 center-of-mass, and μ_R and μ_r are the reduced masses associated with the R and r coordinates, respectively.

We use the DMBE IV potential energy surface (PES) of Pastrana *et al.*[19] on which several quasiclassical,[19,20] quantum mechanical,[13,21−25] and transition state theory[24,26] studies have been carried out. Relative to the asymptotic H(^2S) + $O_2(^3\Sigma_g^-)$ channel, the $HO_2(^2A'')$ well depth is −2.378 35 eV, and the O(^3P) + OH($^2\Pi$) channel is at 0.581 51 eV. The long-range O + OH interaction is dominated by dipole−quadrupole forces,[27] which favor a linear OH···O geometry and culminate in a weakly stable (−0.098 eV) hydrogen-bonded structure at an H···O distance of 3.821 a_0. A shallow barrier, 0.027 eV above the OH···O minimum, precedes the deep HO_2 well, with the H atom rotating out to a HOO angle of 40.2° at the barrier and 104.29° at the HO_2 minimum. No barrier is found between the HO_2 well and H + O_2 products.

A slight adjustment of the DMBE IV PES, involving a simple linear rescaling of the coordinates, has been suggested recently but apparently not used yet.[19] Kendrick and Pack have developed an entirely new multivalued PES[29] intended to better describe the system near conical intersections and permit the study of geometric phase and nonadiabatic effects.[30] We neglect these effects in using the single DMBE IV surface.

B. Basis Set. As in earlier work,[2,22] we employ a discrete variable representation (DVR) basis set of grid points.[31−33] The radial R and r coordinates are represented by equally spaced points appropriate for a sinc function DVR;[34] however, for the present parallel implementation (see below), taking these points as a Fourier grid representation is advantageous. The angular coordinate γ is represented by a Gauss−Legendre DVR, using only odd functions because of the symmetry requirements upon interchange of the two oxygen atoms.[35] We find that a fixed basis size of 64 × 128 × 32 grid points ($R \times r \times \gamma$) is sufficient, with $R \in$[0.1, 7.6] and $r \in$[2, 8]. The restriction to powers of 2 arises from both the Fourier representation and the data-parallel implementation described below.

This grid size corresponds to roughly 20 grid points per thermal de Broglie wavelength,

$$N_B = \frac{2\pi}{\Delta x}\left(\frac{2\mu k_B T}{\hbar^2}\right)^{-1/2} \tag{3.2}$$

at T = 500 K and $N_B \simeq 10$ at T = 2000 K, in both R and r coordinates. (Δx denotes the spacing between grid points.) We

begin to encounter convergence problems with $N_B < 10$, as also observed in earlier applications.[2] We also note the comparable grid size of 60 × 213 × 32 used in the calculation of the cumulative reaction probability $N(E)$ for this reaction.[22]

C. Calculation of Flux Correlation Functions. The correlation functions $C_{rr}(t)$ and $C_{rp}(t)$ are most easily calculated by evaluating the traces in terms of the eigenfunctions of the Boltzmannized (thermal) flux operator[36]

$$\hat{F}_r(\beta) = e^{-\beta\hat{H}/2}\hat{F}_r\, e^{-\beta\hat{H}/2}$$

that is relative to the reactant dividing surface s_r. Denoting the eigenfunctions and corresponding eigenvalues by $|i\rangle$ and λ_i, respectively, we have

$$C_{rr}(t) = \mathrm{Tr}[e^{-\beta\hat{H}/2}\hat{F}_r\, e^{-\beta\hat{H}/2}\, e^{i\hat{H}t/\hbar}\hat{F}_r\, e^{-i\hat{H}t/\hbar}] \tag{3.3a}$$

$$= \sum_i \langle i|e^{-\beta\hat{H}/2}\hat{F}_r\, e^{-\beta\hat{H}/2}\, e^{i\hat{H}t/\hbar}\hat{F}_r\, e^{-i\hat{H}t/\hbar}|i\rangle \tag{3.3b}$$

$$= \sum_i \lambda_i \langle i|e^{i\hat{H}t/\hbar}\hat{F}_r\, e^{-i\hat{H}t/\hbar}|i\rangle \tag{3.3c}$$

$$= \sum_i \lambda_i \langle i(t)|\hat{F}_r|i(t)\rangle \tag{3.3d}$$

where $|i(t)\rangle$ denotes the thermal flux eigenfunction $|i\rangle$ propagated to time t,

$$|i(t)\rangle = e^{-i\hat{H}t/\hbar}|i\rangle \tag{3.4}$$

Similarly,

$$C_{rp}(t) = \sum_i \lambda_i \langle i(t)|\hat{F}_p|i(t)\rangle \tag{3.5}$$

so that both correlation functions are obtained by propagating the same set of thermal flux eigenfunctions.

The Lanczos algorithm[37] is a useful method for finding the largest eigenvalues (and associated eigenvectors) of $\hat{F}_r(\beta)$.[2] Starting with a random initial vector, a Krylov space is formed by successive application of $\hat{F}_r(\beta)$, with complete orthogonalization at each step. Diagonalization of the tridiagonal matrix representation of $\hat{F}_r(\beta)$ in this Krylov basis yields the largest (in absolute value) eigenvalues and their associated eigenvectors. These eigenvalues are monitored at each Lanczos iteration, and the procedure is halted whenever the sum of absolute values of these eigenvalues changes by a small fraction, such as 10^{-4} or 10^{-3}. The eigenvectors in the original coordinate grid representation are then constructed by taking appropriate linear combinations of the Krylov vectors.

As in previous work,[2] we find the most convenient expression for the flux operator to be

$$\hat{F} = \frac{i}{\hbar}[\hat{H}, h(s(\mathbf{q}))] \tag{3.6a}$$

For a dividing surface which is only a function of R and r, this reduces to

$$\hat{F} = \frac{i}{\hbar}[\hat{T}_R, h(s(\mathbf{q}))] + \frac{i}{\hbar}[\hat{T}_r, h(s(\mathbf{q}))] \tag{3.6b}$$

which is readily evaluated in either sinc-DVR or finite difference representations of the 1D operators $\hat{T}_R$ and $\hat{T}_r$.

The (O + OH) reactant dividing surface is chosen at $r = 6.5a_0$, beyond the O−O distance ($r = 5.663a_0$) at the hydrogen-bonded minimum. The H + O_2 product dividing surface is most conveniently defined in terms of either the R Jacobi coordinate (e.g., $R = 6a_0$) or the shortest O−H distance (e.g., $r_{OH} = 3.5a_0$).

D. Time Propagation and Use of Absorbing Potentials. In order to perform the propagation, we use the split operator algorithm.[38] Writing the Hamiltonian in eq 3.1 as

$$\hat{H} = \hat{T}_R + \hat{T}_r + \hat{T}_\gamma + \hat{V} \tag{3.7}$$

we can form the split operator propagator

$$e^{-i(\hat{H}-i\hat{\epsilon})\Delta t/\hbar} \simeq e^{-i(\hat{V}-i\hat{\epsilon})\Delta t/2\hbar}\, e^{-i\hat{T}_\gamma\Delta t/2\hbar}\, e^{-i\hat{T}_R\Delta t/\hbar}\, e^{-i\hat{T}_r\Delta t/\hbar}\, e^{-i\hat{T}_\gamma\Delta t/2\hbar}\, e^{-i(\hat{V}-i\hat{\epsilon})\Delta t/2\hbar} \tag{3.8}$$

The 1D free-particle propagator $e^{-i\hat{T}_R\Delta t/\hbar}$ is applied by using the fast Fourier transform (FFT) to convert from position R to momentum p_R representation, in which the propagator is diagonal, and then a second FFT to return to position space. The $e^{-i\hat{T}_r\Delta t/\hbar}$ term is handled in a similar fashion, while the angular propagator $e^{-i\hat{T}_\gamma\Delta t/\hbar}$ is done using the Gauss−Legendre DVR.

This choice of the split operator expression is determined primarily by (parallel) computational considerations; although the potential referenced expression generally permits a slightly larger time step than the kinetic referenced expression of eq 3.8 under normal circumstances,[39] it would require two applications of each 1D kinetic propagator. Since these terms involve nonlocal operations, from a computational standpoint it is much more desirable to split the localized $\hat{V} - i\hat{\epsilon}$ operator instead. Either way, we would have to split the angular kinetic term $e^{-i\hat{T}_\gamma\Delta t/\hbar}$, but fortunately, the number of angular DVR points required is generally small.

We find that a timestep as long as $\Delta t = 20$ or 30 au (0.5−0.7 fs) is adequate for the real-time propagation, while a slightly smaller time step $\Delta t = 10$ au is generally used for the imaginary-time propagation of the Boltzmann operator $e^{-\beta\hat{H}/2}$.

To avoid unphysical reflection from the boundaries of the DVR grid, we employ absorbing potentials ϵ_τ in each arrangement τ, taken as a function of some coordinate r_τ for each arrangement (see Figure 1). Two convenient choices are the translational Jacobi coordinate for each arrangement, R_τ, or the Jacobi coordinates R and r in which the grid is set up. For the form of the absorbing potentials, the quartic potential has proven to be a robust choice,

$$\epsilon_\tau(r_\tau) = \lambda\left(\frac{r_\tau - r_{0,\tau}}{r_{\max,\tau} - r_{0,\tau}}\right)^4 \tag{3.9}$$

where $r_{0,\tau}$ and $r_{\max,\tau}$ are the starting and ending points of the absorbing potential in the τ arrangement. Typical parameters are $\lambda = 1$ eV and an absorbing potential width of $r_{\max,\tau} - r_{0,\tau} = 1a_0$.

E. Parallel implementation. In order to implement the present method on massively parallel computers, we must first decide the basic quantity to parallelize. In this case, there are two obvious choices: either individual thermal flux eigenfunctions may be placed on separate processors, requiring much interprocessor communication during the Lanczos process but subsequently allowing independent propagation of the thermal flux eigenfunctions, or the DVR grid (i.e., coordinate space itself) may be partitioned among processors. In the former approach, each processor stores (and propagates) one or more complete thermal flux eigenfunctions, while in the latter case each processor contains a segment (corresponding to its portion of coordinate space) of every thermal flux eigenfunction so that the propagations involve a joint effort among processors.

Since we expect (and show below that it is indeed the case) that a relatively small number of thermal flux eigenfunctions is needed, the former approach of assigning a separate eigenfunction to each processor would be limited to a number of processors equal to the number of eigenfunctions, whereas we would hope to take full advantage of the 128 or 256 processors commonly available on most massively parallel computer systems. Thus, we adopt the latter perspective and partition *coordinate space* among processors.

In order to proceed in this manner, we must minimize the interprocessor communication required during application of the flux and Hamiltonian propagation operators. Since the potential operator is entirely local in the DVR grid basis, the only remaining question is the kinetic operators. In previous work on the parallel implementation of direct cumulative reaction probability calculations,[40] we have found a five- or seven-point finite difference representation of the second derivative terms rather than the full-fledged sinc function DVR,[34] to provide an adequate balance between data locality and accuracy for radial degrees of freedom. A seven-point finite difference approximation is thus used for the $\hat{T}_R$ and $\hat{T}_r$ operators in eq 3.6b.

However, for the time evolution part of the calculation, the necessary time step for finite-difference schemes is too short to be of practical use. Instead, we have chosen the fast Fourier Transform (FFT) approach to switch between coordinate and momentum representations, as described following eq 3.8. Although the FFT approach, like the sinc-function DVR, requires an "all-to-all" communication across the *R* and *r* degrees of freedom and thus is highly nonlocal, FFT algorithms are inherently parallel[41] and thus can be quite efficient for our purposes. (This is only true for densely connected architectures, in particular hypercube networks; communication bottlenecks may arise on loosely connected architectures such as rings and meshes.)

F. Reactant Partition Functions. The $H(^2S) + O_2(^3\Sigma_g^-)$ partition function is given by

$$Q_r(T) = Q_{elec}Q_{vib}Q_{rot}Q_{trans} \tag{3.10}$$

where $Q_{elec} = {}^6/_2$ is the electronic degeneracy divided by the two equivalent arrangements (since the Gauss−Legendre DVR is restricted to one half-plane), Q_{vib} and Q_{rot} are the usual vibrational and rotational partition functions, and $Q_{trans} = (\mu k_B T/(2\pi\hbar^2))^{3/2}$ is the translational partition function per unit volume for the relative motion of H and O_2.

The $O(^3P) + OH(^2\Pi)$ partition function also includes electronic factors accounting for the $^3P_{2,1,0}$ spin−orbit states of O and the $^2\Pi_{3/2,1/2}$ OH spin doublet:[27,42]

$$Q_{elec}^{O}Q_{elec}^{OH} = [5 + 3\,e^{-228K/T} + e^{-326K/T}][2 + 2\,e^{-205K/T}] \tag{3.11}$$

However, the OH rotational partition function is somewhat problematic, since at low energies the coupling of spin and orbital angular momenta is best described by Hund's case a, while higher rotational energy levels are more nearly approximated by case b.[43] We have computed rovibrational partition functions using either case a, involving half-integral rotational quantum numbers *j*, or case b, with integral quantum numbers $N = 1, 2, 3, \ldots$ Since these results differ by a few percent, the rate constants reported below use a simpler, albeit indirect approach: dividing the $H + O_2$ partition function by the $H + O_2 \rightarrow O + OH$ equilibrium constant, which is given within a tenth of a percent over the temperature range of interest by the expression[44]

$$K_{eq}(T) = 2.7 \times 10^{-3} T^{0.4}\, e^{8720K/T} \tag{3.12}$$

An additional reason for taking this indirect approach is that the $O(^3P) + OH(^2\Pi)$ reactants correlate with both the $^2A''$ ground surface and $^2A'$ first excited surface of HO_2, which in turn correlate with the $H(^2S) + O_2(^3\Sigma_g^-)$ and $H(^2S) + O_2(^1\Delta_g)$ products, respectively. At high enough temperatures (probably including those considered here), this singlet oxygen channel via $HO_2(^2A')$ can become significant and must be taken into account.[45,46] Since this is beyond the scope of the present work, we adopt the above approach of using the experimental equilibrium constant to define an effective partition function for the O + OH reactants.

G. *J*-Shifting. In the *J*-shifting approximation,[17] it is assumed that the overall rotation is decoupled from internal motion and, therefore, that its effect is merely to add a constant rotational energy term ϵ_{rot}^{JK} to the $J = 0$ Hamiltonian of eq 3.1. For thermal rate constants, this corresponds to the multiplication of the $J = 0$ rate by an additional rotational partition function for the entire complex,

$$Q_{rot}^{\ddagger} = \sum_{J=0}^{\infty}(2J+1)\sum_{K=-J}^{J} e^{-\beta\epsilon_{rot}^{JK}} \tag{3.13}$$

We estimate the rotational energies ϵ_{rot}^{JK} by treating the HO_2 complex as a rigid rotor fixed at its equilibrium geometry, with rotational constants $A^{\ddagger} = 18.94\ cm^{-1}$, $B^{\ddagger} = 0.589\ cm^{-1}$, and $C^{\ddagger} = 0.572\ cm^{-1}$. Nearly identical results are obtained using either the classical expression for $Q_{rot}^{\ddagger}$,

$$Q_{rot}^{\ddagger} \simeq \left(\frac{\pi(k_B T)^3}{A^{\ddagger}B^{\ddagger}C^{\ddagger}}\right)^{1/2} \tag{3.14}$$

or numerical evaluation of eq 3.13 with symmetric top rotational constants $A^{\ddagger}$ and $\bar{B}^{\ddagger} = (B^{\ddagger} + C^{\ddagger})/2$. At $T = 500$ and 2000 K, the sum over the total angular momentum in eq 3.13 must run to $J = 52$ and 105, respectively, in order to obtain 99% of the total. The large $Q_{rot}^{\ddagger}(T)$ values, ranging from 4549 to 36 375 over this temperature range, also indicate how miniscule the $J = 0$ contribution is and, thus, how important it is to have an accurate estimate of the $J > 0$ contributions.

IV. Results and Discussion

A. Thermal Flux Eigenfunctions. The required computational effort will be proportional to two factors: the number of thermal flux eigenvectors that must be propagated and the amount of propagation time required. Owing to the large number of HO_2 bound states and resonances, we anticipate a large propagation time; we will return to this issue below.

In one dimension, the thermal flux operator has only two nonzero eigenvalues, one positive and one negative, with identical magnitudes, corresponding to flux in the forward and backward directions.[36] Additional degrees of freedom lead to a set of activated complex states in the transition state theory picture; the nonzero eigenvalues still occur in pairs, one for each accessible state of the activated complex. Figure 3 shows the magnitudes of these eigenvalues for several temperatures relative to the largest eigenvalue at each temperature. The number of eigenvalue pairs required is seen to increase from 10 or 12 at $T = 600$ K to nearly 25 at $T = 2000$ K. Thus, the total number of eigenfunctions that must be propagated is 20−50, not a great deal more than is often required. If a much greater number were necessary, it would make sense to employ a different parallelization scheme and do the *propagations*

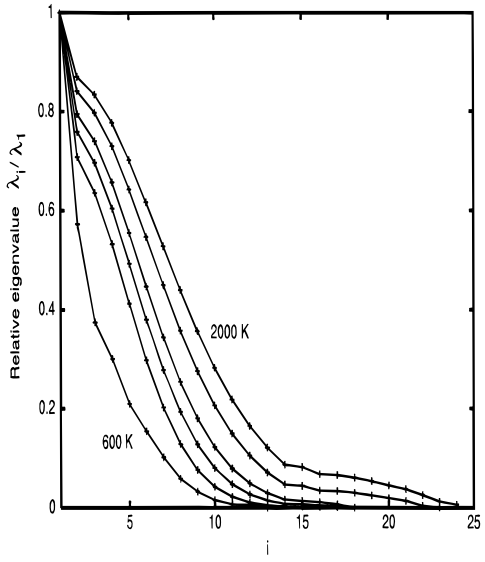

Figure 3. Positive thermal flux eigenvalues for $T = 600$, 800, 1000, 1200, 1600, and 2000 K. Note that the eigenvalues occur in ± pairs so that the actual number of eigenvalues required is twice that shown.

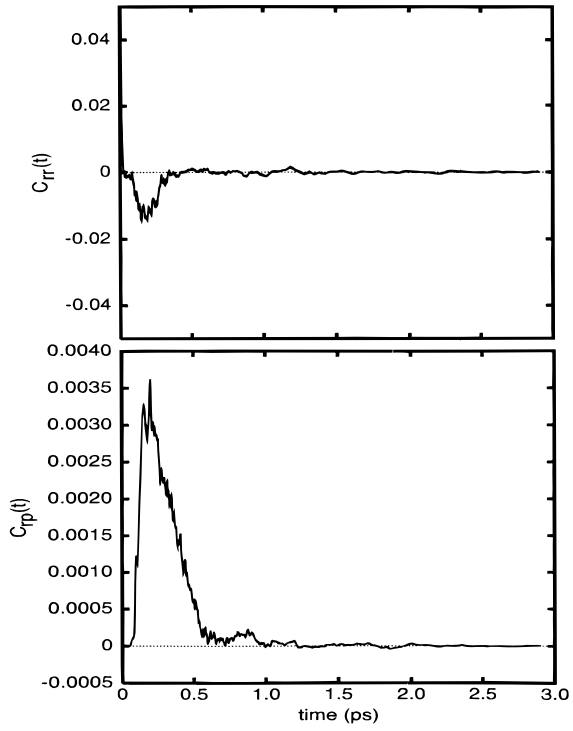

Figure 4. Flux−flux correlation functions $C_{rr}(t)$ (top panel) and $C_{rp}(t)$ (bottom panel) for the OH + O → H + O_2 reaction at $T = 1200$ K. Both correlation functions are shown relative to the reactant flux autocorrelation function at zero time, $C_{rr}(0)$.

separately on different processors rather than dividing each *wave function* among processors.

B. Flux−Flux Correlation Functions. The flux−flux autocorrelation function $C_{rr}(t)$ and cross-correlation function $C_{rp}(t)$ are shown in Figure 4 for $T = 1200$ K. Both correlation functions are scaled by $C_{rr}(0)$; the initial decay of the autocorrelation function occurs within a few femtoseconds ($\sim\hbar\beta \simeq 6$ fs),[7] so the plot of $C_{rr}(t)$ is magnified to show the subsequent oscillations. A significant amount of recrossing is observed, with a highly structured negative lobe lasting for approximately 300 fs, followed by smaller positive and negative lobes corresponding to breakup of the metastable HO_2 complex into products and reactants, respectively.

This recrossing fraction can be quantified by comparing the area under the initial positive lobe (up to the first zero at t_0) with the total area

$$\kappa(T) = \frac{\int_0^\infty dt\, C_{rr}(t)}{\int_0^{t_0} dt\, C_{rr}(t)} \tag{4.1}$$

This is readily identified as the transmission coefficient correction to the quantum transition state theory proposed by Tromp and Miller,[47] which relates the thermal rate constant to the area under the initial positive lobe of the flux autocorrelation function,

$$k_{QMTST}(T) = [Q_r(T)]^{-1} \int_0^{t_0} dt\, C_{rr}(t) \tag{4.2}$$

so that the true quantum rate constant is $k(T) = \kappa(T) k_{QMTST}(T)$. From the $T = 1200$ K autocorrelation function in Figure 4, we find $\kappa \simeq 0.310$, meaning that 69% of the initial flux into the complex region recrosses back to reactants. This of course is dependent upon the position of the reactant-dividing surface, but similar values are obtained for several reasonable choices. As the temperature is increased, κ increases slightly and t_0 decreases slightly. Miller has found a similar recrossing fraction in his quasiclassical trajectory calculations, where 60−68% of the HO_2^* complexes recross to give O + OH reactants over the 500−2000 K temperature range considered here.[48]

(The even larger recrossing for the H + O_2 reactants, >99%, causes enormous cancellation in the time integral of $C_{rr}(t)$ for this direction. The magnitude of $\kappa(T)$ for this uphill reaction can be estimated by the Boltzmann factor $e^{-\beta\Delta E}$, which is roughly 10^{-6} at 500 K and ~0.03 at 2000 K. Therefore, the present work is limited to the study of O + OH + M reaction and recombination and does not consider that of H + O_2 + M.)

The cross-correlation function is initially zero, until the propagated (reactant) thermal flux eigenfunctions reach the product dividing surface and a large positive lobe occurs, lasting several hundred femtoseconds. Since a negative contribution to $C_{rp}(t)$ corresponds to the unlikely event of H + O_2 products "turning around" and re-entering the HO_2 complex region, no such lobe is expected, nor is one observed.

C. Thermal Rate Constants. From eqs 2.9a and 2.9b, the $J = 0$ thermal rate constant may be obtained from the time integrals of either $C_{rr}(t)$ or $C_{rp}(t)$, as shown in Figure 5. As expected, the abundant recrossing in the autocorrelation function leads to a great deal of cancellation in the time integral, while the integral of the cross-correlation function increases nearly monotonically. This seems to suggest that use of $C_{rp}(t)$ may be a more efficient approach to the thermal rate constant for cases where significant recrossing in $C_{rr}(t)$ occurs. At 1 ps the two rates agree with each other (and with the final converged rates) to a few percent, probably the ultimate accuracy obtainable with such calculations. All calculations reported here have been propagated a bit further, to 3 or 4 ps, to lessen the discrepancy between eqs 2.9a and 2.9b.

As a check of the validity of using the thermal flux eigenvalues as a measure of the number of required eigenvectors, Figure 6 shows the $J = 0$ rate constant versus number of Lanczos iterations (or equivalently, number of thermal flux eigenfunctions) at $T = 1000$ K. The rate (computed from either $C_{rr}(t)$ or $C_{rp}(t)$) appears to converge with around 30 iterations, in good agreement with the 15 pairs of significant eigenvalues in Figure 3.

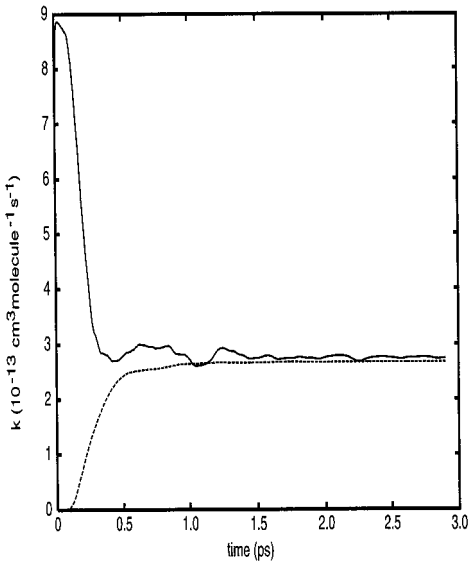

Figure 5. Convergence of the $J = 0$ thermal rate constant ($T = 1200$ K) versus time for the two flux−flux correlation functions shown in Figure 4. The solid curve is for $C_{rr}(t)$ and the dashed curve for $C_{rp}(t)$.

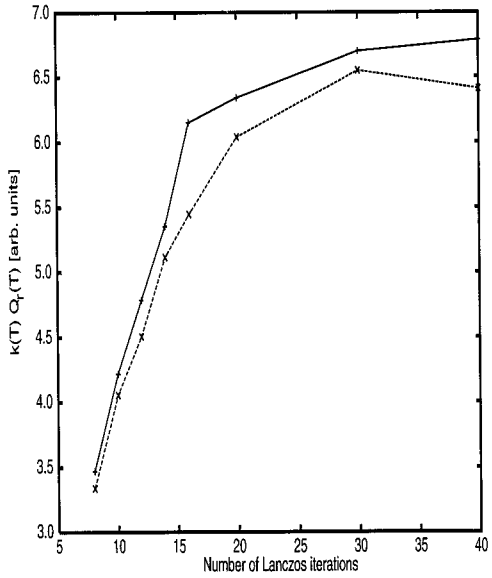

Figure 6. Convergence of the $J = 0$ thermal rate constant ($T = 1000$ K) with respect to the number of thermal flux eigenvalues used in the calculation (i.e., the number of Lanczos iterations). Rate constants computed from both $C_{rr}(t)$ (dashed) are shown.

TABLE 1: Thermal Rate Constants for the Forward and Reverse Three-Dimensional H + O_2 ⇌ O + OH Reactions in Units of cm^3 molecule^{-1} s^{-1}

T (K)	k_1 (T)	k_{-1} (T)
500	1.50 (−17)[a]	1.83 (−11)
600	2.65 (−16)	1.89 (−11)
700	1.88 (−15)	1.80 (−11)
800	8.24 (−15)	1.74 (−11)
1000	6.66 (−14)	1.74 (−11)
1200	2.71 (−13)	1.78 (−11)
1500	1.10 (−12)	1.85 (−11)
2000	4.48 (−12)	1.98 (−11)

[a] The number in parentheses is the power of 10.

Using the *J*-shifting approximation and eq 3.12 for the thermal equilibrium constant, we obtain the forward and reverse thermal rate constants listed in Table 1. We find that the rate constants computed from the autocorrelation function $C_{rr}(t)$ are generally 2−5% greater than those from the cross-correlation functions $C_{rp}(t)$; the results in Table 1 are mean values.

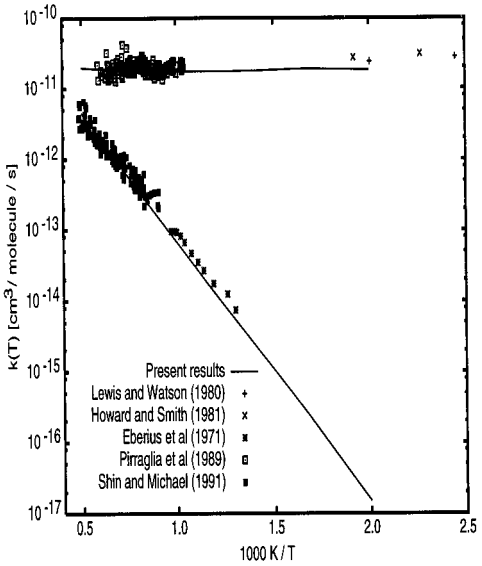

Figure 7. Arrhenius plot of calculated and experimental thermal rate constants for the forward and reverse reactions. Present results (Table 1) are shown as a solid line, while the different symbols refer to different experiments as indicated in the legend. To reduce clutter, the O + OH rate constants reported by Pirraglia et al.[50] are shown, although their actual rate measurements are for the H + O_2 reaction.

In Figure 7 we compare our thermal rate constants with experimentally measured rates for the H + O_2 (refs 49−51) and O + OH (refs 52 and 53) reactions. Good agreement is found over the entire temperature range, with the high-temperature calculations lying in the middle of the widely scattered experimental measurements. At lower temperatures, the present results underestimate the experimental rates (which are known quite accurately). Whether this is due to the *J*-shifting approximation or deficiencies in the potential energy surface (including its treatment as a single electronic surface) is unknown. At temperatures below 500 K, we have been unable to obtain converged thermal eigenvalues and eigenfunctions; these numerical difficulties are evident at 500 K but are unlikely to account for the entire discrepancy between experimental and calculated rates.

D. Recombination Rates. In order to convert from the collision frequency ω to a more familiar variable such as pressure P, we approximate the collisional deactivation rate constant by the hard sphere collision theory expression $\sigma\bar{v}$, and also using the ideal gas expression for [M] yields

$$\omega = k_{\text{deact}}[\text{M}] = \sigma\sqrt{\frac{8k_{\text{B}}T}{\pi\mu}}\left(\frac{P}{kT}\right) \tag{4.3}$$

By use of a typical cross section $\sigma = 10$ Å^2 and introducing the appropriate conversion factors, this gives

$$\omega = 10^{-6}P\sqrt{\frac{11112/\mu}{T}} \tag{4.4}$$

with ω in fs^{-1}, P in atm, μ in atomic units, and T in K. The factor $11112/\mu$ with various collision partners for HO_2 varies from 413 for SF_6 and 615 for Ar, to 3115 for He and 5893 for H_2, so we choose an intermediate value of 2000 as a first approximation

$$\omega = 10^{-6}P\sqrt{\frac{2000}{T}} \tag{4.5}$$

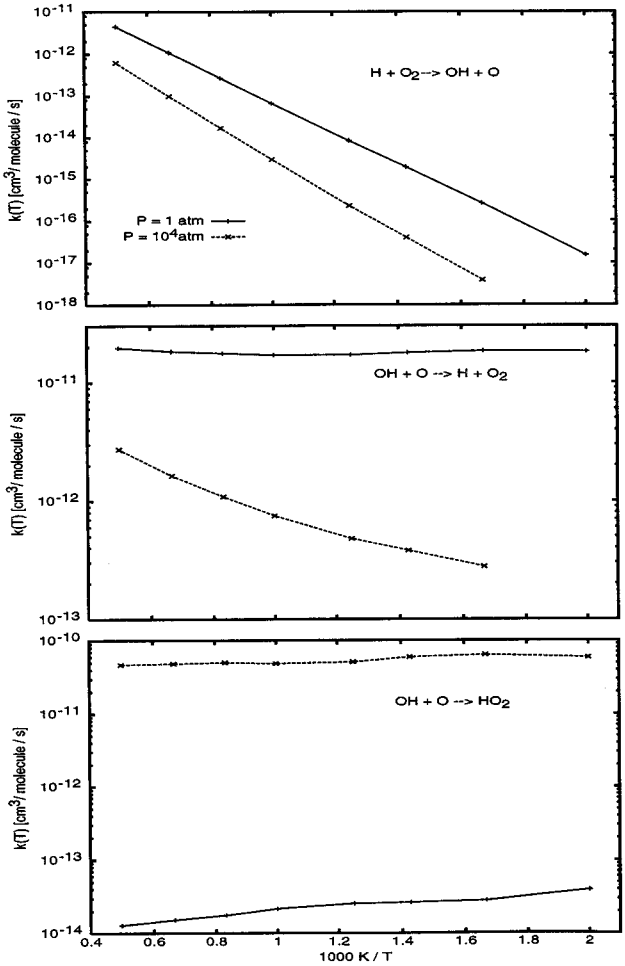

Figure 8. Arrhenius plot of calculated reaction and recombination rate for $P = 1$ and 10^4 atm.

The effect of collisional recombination on the thermal reaction and recombination rates is shown in Arrhenius form in Figure 8 and as pressure-dependent fall-off curves in Figure 9. To our knowledge, there are no experimental data for the O + OH + M system with which to compare, although H + O_2 + M → HO_2 + M fall-off curves have been measured for several third-body species M. In addition to O + OH + M → HO_2 + M fall-off curves, high-pressure measurements of the reaction rates (in either direction) would provide a useful test of this theory; our results suggest that dampening of the forward and reverse reaction rates due to collisional recombination should become significant for pressures around 1000 atm.

On the theoretical side, H + O_2 + M → HO_2 + M recombination has been studied quantum mechanically by Mandelshtam *et al.*,[13] and RRKM calculations have recently been reported for this system by Duchovic and co-workers.[54] However, both studies have focused on the recombination rate (Mandelshtam *et al.*[13] specifically examined only energies below the O + OH threshold), whereas we are able to study the competition between both reaction and recombination for the reverse O + OH + M system.

V. Concluding Remarks

We have extended a recently proposed theory for unimolecular recombination rates[8] to treat chemical reactions that proceed via a collision complex that may be stabilized. This theory has been implemented within the framework of flux−flux correlation function approaches to thermal rate constants and demonstrated for the O + OH → H + O_2, HO_2 system.

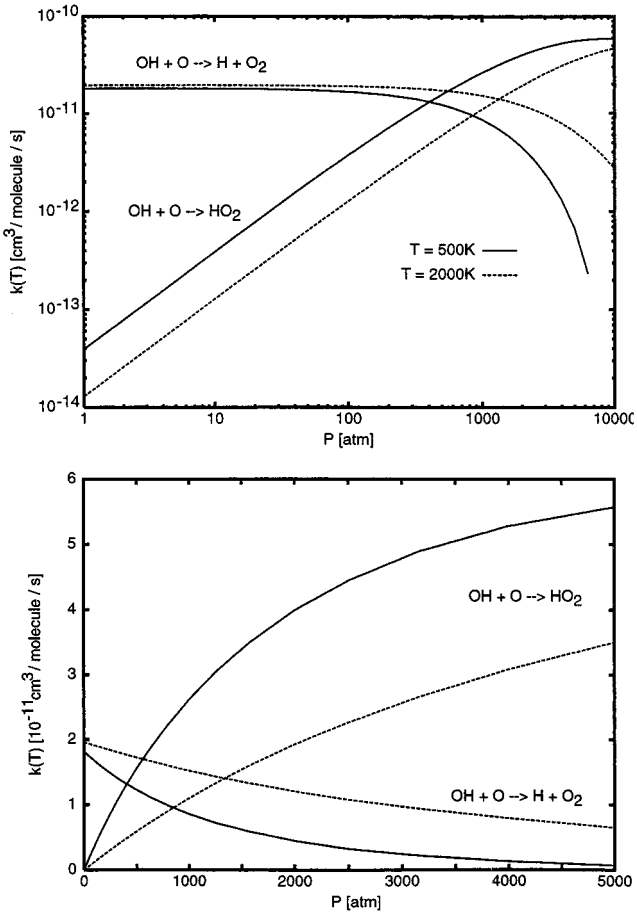

Figure 9. Pressure-dependent fall-off curves of the O + OH reaction and recombination rates for $T = 500$ and 2000 K.

By taking advantage of current massively parallel computers (most calculations here were carried out on 64- or 128-node Cray T3D partitions), we were able to carry out the necessary long-time propagation (2−3 ps) of the thermal flux eigenfunctions. Our current parallel implementation uses a spatial decomposition, with the large DVR grid (64 × 128 × 32) partitioned among processors. Improved performance can be expected with a mixed approach in which both thermal flux eigenfunctions and coordinate space are partitioned.[55] For instance, a calculation using 64 processor nodes for the propagation of 8 wave functions could dedicate each node to 1/8th of *one* wave function instead of each node handling 1/64th of *every* wave function.

We have seen that even in the absence of recombination, the cross-correlation function $C_{rp}(t)$ may provide a useful method for computing thermal rate constants in the presence of deep intermediate wells. Another suggested approach[56] has been to take the $\omega \rightarrow 0$ limit of the autocorrelation function integral with an exponential damping factor $e^{-\omega t}$,

$$k_{p\leftarrow r}(T) = [Q_r(T)]^{-1} \lim_{\omega \rightarrow 0} \int_0^\infty dt\, e^{-\omega t}\, C_{rr}(t) \qquad (5.1)$$

which our analysis in section II would interpret as the zero-pressure limit of $k_{recomb}(T) + k_{p\leftarrow r}(T)$.

Given the great dependence on the *J*-shifting approximation for extrapolation of the $J = 0$ reaction and recombination rates, and its questionable validity in the present case of a deep well, rather than a transition state barrier, $J > 0$ calculations would be of great benefit. Since *J* values as high as 50 or 100 contribute significantly to the total rate, calculations for all (*J*, *K*) are clearly unfeasible, even if these calculations assume a

simplified model such as the helicity conserving approximation. However, one may compute rates for only a few selected (J, K) values and obtain approximate rates for all other (J, K) by interpolation.[2]

Acknowledgment. We thank Professor Claude Leforestier for providing the DMBE IV potential subroutine, and Dr. Ward H. Thompson for numerous discussions. This work was supported by the Director, Office of Energy Research, Office of Basic Energy Sciences, Chemical Sciences Division of the U.S. Department of Energy under Contract No. DE-AC03-76SF00098, and by a grant of Cray T3D computer time from the Advanced Computing Initiative in Science and Engineering (ACISE) at the Lawrence Livermore National Laboratory (LLNL), and by the National Science Foundation Grant CHE94−22559. T.C.G. gratefully acknowledges a research fellowship from the Miller Institute for Basic Research in Science.

Appendix A: Alternate Forms of the Rate Expressions

In this appendix we give formulas for the thermal recombination and reaction rates in terms of the eigenfunctions $\{\Psi_l\}$ and eigenvalues $\{E_l - i\Gamma_l/2\}$ of $\hat{H} - i\hat{\epsilon}$. By introduction of these eigenfunctions as a basis, the integrals in eqs 2.6a and 2.6b may be written as

$$\int_0^\infty \mathrm{d}t\, \mathrm{e}^{-\omega t} C_{s,s'} = \sum_{l,l'} \mathrm{e}^{-\beta(E_l+E_{l'})/2} \frac{\langle \Psi_l|\hat{F}_s|\Psi_{l'}^*\rangle\langle \Psi_{l'}^*|\hat{F}_{s'}|\Psi_l\rangle}{\omega + \dfrac{\Gamma_l + \Gamma_{l'}}{2\hbar} + \dfrac{\mathrm{i}}{\hbar}(E_l - E_{l'})} \quad \text{(A1)}$$

where s and s' may be either r or p. Using the commutator expression for the flux operator,

$$\hat{F}_\mathrm{s} = \frac{\mathrm{i}}{\hbar}[\hat{H}, \hat{h}_\mathrm{s}]$$

the flux terms in eq A1 can be expressed as

$$\langle \Psi_{l'}^*|\hat{F}_{s'}|\Psi_l\rangle = -\left[\frac{\Gamma_l + \Gamma_{l'}}{2\hbar} + \frac{\mathrm{i}}{\hbar}(E_l - E_{l'})\right]\langle \Psi_{l'}^*|\hat{h}_\mathrm{s}|\Psi_l\rangle + \frac{2}{\hbar}\langle \Psi_{l'}^*|\hat{\epsilon}_\mathrm{p}|\Psi_l\rangle \quad \text{(A2)}$$

References and Notes

(1) (a) Jaquet, R.; Miller, W. H. *J. Phys. Chem.* **1985**, *89*, 2139. (b) Yamashita, K.; Miller, W. H. *J. Chem. Phys.* **1985**, *82*, 5475. (c) Tromp, J. W.; Miller, W. H. *J. Phys. Chem.* **1986**, *90*, 3482. (d) Tromp, J. W.; Miller, W. H. *Faraday Discuss., Chem. Soc.* **1987**, *84*, 441. (e) Makri, N.; Miller, W. H. *J. Chem. Phys.* **1989**, *90*, 904.

(2) (a) Thompson, W. H.; Miller, W. H. *J. Chem. Phys.* **1995**, *102*, 9205. (b) Thompson, W. H.; Miller, W. H. *J. Chem. Phys.* **1997**, *106*, 142.

(3) (a) Park, T. J.; Light, J. C. *J. Chem. Phys.* **1986**, *85*, 5870. (b) Park, T. J.; Light, J. C. *J. Chem. Phys.* **1988**, *88*, 4897. (c) Park, T. J.; Light, J. C. *J. Chem. Phys.* **1989**, *91*, 974. (d) Park, T. J.; Light, J. C. *J. Chem. Phys.* **1991**, *94*, 2946. (e) Park, T. J.; Light, J. C. *J. Chem. Phys.* **1992**, *96*, 8853. (f) Brown, D.; Light, J. C. *J. Chem. Phys.* **1992**, *97*, 5465.

(4) Day, P. N.; Truhlar, D. G. *J. Chem. Phys.* **1991**, *94*, 2045.

(5) Manthe, U. *J. Chem. Phys.* **1995**, *102*, 9205.

(6) Yamamoto, T. *J. Chem. Phys.* **1960**, *33*, 281.

(7) Miller, W. H.; Schwartz, S. D.; Tromp, J. W. *J. Chem. Phys.* **1983**, *79*, 4889.

(8) Miller, W. H. *J. Phys. Chem.* **1995**, *99*, 12387.

(9) (a) Robinson, P. J.; Holbrook, K. A. *Unimolecular Reactions*; Wiley: New York, 1972. (b) Forst, W. *Theory of Unimolecular Reactions*; Academic Press: New York, 1973. (c) Gilbert, R. G.; Smith, S. C. *Theory of Unimolecular and Recombination Reactions*; Blackwell: Oxford, 1990.

(10) Miller, W. H. *Faraday Discuss., Chem. Soc.* **1995**, *102*, 53.

(11) Kendrick, B.; Pack, R. T. *Chem. Phys. Lett.* **1995**, *235*, 291.

(12) Qi, J.; Bowman, J. M. *J. Phys. Chem.* **1996**, *100*, 15165.

(13) Mandelshtam, V. A.; Taylor, H. S.; Miller, W. H. *J. Chem. Phys.* **1996**, *105*, 496.

(14) Miller, J. A.; Kee, R. J.; Westbrook, C. K. *Annu. Rev. Phys. Chem.* **1990**, *41*, 345.

(15) See, for example, the following. Pilling, M. J.; Seakins, P. W. *Reaction Kinetics*; Oxford University Press: Oxford, 1995; Chapter 10.

(16) Wennberg, P. O.; Cohen, R. C.; Stimpfle, R. M.; Koplow, J. P.; Anderson, J. G.; Salawitch, R. J.; Fahey, D. W.; Woodbridge, E. L.; Keim, E. R.; Gao, R. S.; Webster, C. R.; May, R. D.; Toohey, D. W.; Avallone, L. M.; Proffitt, M. H.; Loewenstein, M.; Podolske, J. R.; Chan, K. R.; Wofsy, S. C. *Science* **1994**, *266*, 398.

(17) Bowman, J. M. *J. Phys. Chem.* **1991**, *95*, 4960.

(18) See, for example, the following. Troe, J. *J. Chem. Phys.* **1982**, *77*, 3485.

(19) Pastrana, M. R.; Quintales, L. A. M.; Brandão, J.; Varandas, A. J. C. *J. Phys. Chem.* **1990**, *94*, 8073.

(20) (a) Varandas, A. J. C.; Brandão, J.; Pastrana, M. R. *J. Chem. Phys.* **1992**, *96*, 5137. (b) Varandas, A. J. C. *J. Chem. Phys.* **1993**, *99*, 1076.

(21) (a) Pack, R. T.; Butcher, E. A.; Parker, G. A. *J. Chem. Phys.* **1993**, *99*, 9310. (b) Pack, R. T.; Butcher, E. A.; Parker, G. A. *J. Chem. Phys.* **1995**, *102*, 5998.

(22) Leforestier, C.; Miller, W. H. *J. Chem. Phys.* **1994**, *100*, 733.

(23) (a) Zhang, D. H.; Zhang, J. Z. H. *J. Chem. Phys.* **1994**, *101*, 3671. (b) Dai, J.; Zhang, J. Z. H. *J. Chem. Phys.* **1996**, *104*, 3664. (c) Dai, J.; Zhang, J. Z. H. *J. Phys. Chem.* **1996**, *100*, 6898.

(24) (a) Dobbyn, A. J.; Stumpf, M.; Keller, H.-M.; Hase, W. L.; Schinke, R. *J. Chem. Phys.* **1995**, *102*, 5867. (b) Song, K.; Peslherbe, G. H.; Hase, W. L.; Dobbyn, A. J.; Stumpf, M.; Schinke, R. *J. Chem. Phys.* **1995**, *103*, 8891. (c) Dobbyn, A. J.; Stumpf, M.; Keller, H.-M.; Schinke, R. *J. Chem. Phys.* **1995**, *103*, 9947. (d) Dobbyn, A. J.; Stumpf, M.; Keller, H.-M.; Schinke, R. *J. Chem. Phys.* **1996**, *104*, 8357.

(25) Mandelshtam, V. A.; Grozdanov, T. P.; Taylor, H. S. *J. Chem. Phys.* **1995**, *103*, 10074.

(26) Yang, C.-Y.; Klippenstein, S. J. *J. Chem. Phys.* **1995**, *103*, 7287.

(27) Graff, M. M.; Wagner, A. F. *J. Chem. Phys.* **1990**, *92*, 2423.

(28) Varandas, A. J. C.; Bowman, J. M.; Gazdy, B. *Chem. Phys. Lett.* **1995**, *233*, 405.

(29) Kendrick, B.; Pack, R. T. *J. Chem. Phys.* **1995**, *102*, 1994.

(30) (a) Kendrick, B.; Pack, R. T. *J. Chem. Phys.* **1996**, *104*, 7475. (b) Kendrick, B.; Pack, R. T. *J. Chem. Phys.* **1996**, *104*, 7502.

(31) Dickinson, A. S.; Certain, P. R. *J. Chem. Phys.* **1963**, *49*, 4209.

(32) Harris, D. O.; Engerholm, G. G.; Gwinn, W. D. *J. Chem. Phys.* **1965**, *43*, 1515.

(33) (a) Lill, J. V.; Parker, G. A.; Light, J. C. *Chem. Phys. Lett.* **1982**, *89*, 483. (b) Light, J. C.; Hamilton, I. P.; Lill, J. V. *J. Chem. Phys.* **1985**, *82*, 1400. (c) Lill, J. V.; Parker, G. A.; Light, J. C. *J. Chem. Phys.* **1986**, *85*, 900. (d) Bačić, Z.; Light, J. C. *J. Chem. Phys.* **1986**, *85*, 4594. (e) Whitnell, R. M.; Light, J. C. *J. Chem. Phys.* **1988**, *89*, 3674. (f) Choi, S. E.; Light, J. C. *J. Chem. Phys.* **1990**, *92*, 2129.

(34) Colbert, D. T.; Miller, W. H. *J. Chem. Phys.* **1992**, *96*, 1982.

(35) The symmetry analysis is much less straightforward when the C_{2v} conical intersection is taken into account; see Barclay, V. J.; Dateo, C. E.; Hamilton, I. P.; Kendrick, B.; Pack, R. T.; Schwenke, D. W. *J. Chem. Phys.* **1995**, *103*, 3864.

(36) Park, T. J.; Light, J. C. *J. Chem. Phys.* **1988**, *88*, 4897.

(37) Lanczos, C. *J. Res. Natl. Bur. Stand.* **1950**, *45*, 255.

(38) (a) Fleck, J. A., Jr.; Morris, J. R.; Feit, M. D. *Appl. Phys.* **1976**, *10*, 129. (b) Feit, M. D.; Fleck, J. A., Jr.; Steiger, A. *J. Comput. Phys.* **1982**, *47*, 412.

(39) Truong, T. N.; Tanner, J. J.; Bala, P.; McCammon, J. A.; Kouri, D. J.; Lesyng, B.; Hoffman, D. K. *J. Chem. Phys.* **1992**, *96*, 2077.

(40) Germann, T. C.; Miller, W. H. Unpublished results.

(41) Boghosian, B. M.; Hillis, W. D. *Science* **1993**, *261*, 856.

(42) Clary, D. C.; Werner, H.-J. *Chem. Phys. Lett.* **1984**, *112*, 346.

(43) Alexander, M. H. *J. Chem. Phys.* **1982**, *76*, 5974.

(44) Cohen, N.; Westberg, K. R. *J. Phys. Chem. Ref. Data* **1983**, *12*, 531.

(45) Troe, J. *Twenty-Second Symposium (International) on Combustion*; The Combustion Institute: Pittsburgh, 1988; p 843.

(46) Du, H.; Hessler, J. P. *J. Chem. Phys.* **1992**, *96*, 1077.

(47) Tromp, J. W.; Miller, W. H. *J. Phys. Chem.* **1986**, *90*, 3482.

(48) Miller, J. A. *J. Chem. Phys.* **1986**, *84*, 6170.

(49) Eberius, K. H.; Hoyermann, K.; Wagner, H. Gg. *Thirteenth Symposium (International) on Combustion*; The Combustion Institute: Pittsburgh, 1971; p 713.

(50) Pirraglia, A. N.; Michael, J. V.; Sutherland, J. W.; Klemm, R. B. *J. Phys. Chem.* **1989**, *93*, 282.

(51) Shin, K. S.; Michael, J. V. *J. Chem. Phys.* **1991**, *95*, 262.

(52) Lewis, R. S.; Watson, R. T. *J. Phys. Chem.* **1980**, *84*, 3495.
(53) Howard, M. J.; Smith, I. W. M. *J. Chem. Soc., Faraday Trans. 2* **1981**, *77*, 997.
(54) Duchovic, R. J.; Pettigrew, J. D.; Welling, B.; Shipchandler, T. *J. Chem. Phys.* **1996**, *105*, 10367.
(55) Wiggs, J.; Jónsson, H. *Comput. Phys. Commun.* **1995**, *87*, 319.
(56) Thachuk, M.; Mayne, H. R.; Schatz, G. C. *J. Chem. Phys.* **1993**, *99*, 3516.